





Review

Laser Coatings via State-of-the-Art Additive Manufacturing: A Review

Muhammad Arif Mahmood ^{1,2} , Alexandra Bănică ^{1,3} , Carmen Ristoscu ¹ , Nicu Becherescu ⁴ and Ion N. Mihăilescu ^{1,*} 

¹ Laser Department, National Institute for Laser, Plasma and Radiation Physics (INFLPR), Magurele, 077125 Ilfov, Romania; arif.mahmood@inflpr.ro (M.A.M.); alexandra.banica@inflpr.ro (A.B.); carmen.ristoscu@inflpr.ro (C.R.)

² Faculty of Physics, University of Bucharest, Magurele, 077125 Ilfov, Romania

³ Faculty of Medicine, Carol Davila University of Medicine and Pharmacy, 02002 Bucharest, Romania

⁴ S.C. Apel Laser S.R.L., 25 Vanatorilor Street, Mogosoia, 077135 Ilfov, Romania; becherescu@gmail.com

* Correspondence: ion.mihailescu@inflpr.ro; Tel.: +40-21-4574491

Abstract: Ceramics and ceramic-reinforced metal matrix composites (CMMCs) demonstrate high wear resistance, excellent chemical inertness, and exceptional properties at elevated temperatures. These characteristics are suitable for their utilization in biomedical, aerospace, electronics, and other high-end engineering industries. The aforementioned performances make them difficult to fabricate via conventional manufacturing methods, requiring high costs and energy consumption. To overcome these issues, laser additive manufacturing (LAM) techniques, with high-power laser beams, were developed and extensively employed for processing ceramics and ceramic-reinforced CMMCs-based coatings. In respect to other LAM processes, laser melting deposition (LMD) excels in several aspects, such as high coating efficiency and lower labor cost. Nevertheless, difficulties such as poor bonding between coating and substrate, cracking, and reduced toughness are still encountered in some LMD coatings. In this article, we review recent developments in the LMD of ceramics and CMMCs-based coatings. Issues and solutions, along with development trends, are discussed and summarized in support of implementing this technology for current industrial use.

Keywords: 3D printing; laser melting deposition; ceramic-based coatings; ceramic-reinforced metal matrix composite-based coatings; properties of coatings; potential problems and their solutions for coatings by laser melting deposition



Citation: Mahmood, M.A.; Bănică, A.; Ristoscu, C.; Becherescu, N.; Mihăilescu, I.N. Laser Coatings via State-of-the-Art Additive Manufacturing: A Review. *Coatings* **2021**, *11*, 296. <https://doi.org/10.3390/coatings11030296>

Academic Editor: Chang-Hwan Choi

Received: 8 February 2021

Accepted: 27 February 2021

Published: 4 March 2021

Publisher's Note: MDPI stays neutral with regard to jurisdictional claims in published maps and institutional affiliations.



Copyright: © 2021 by the authors. Licensee MDPI, Basel, Switzerland. This article is an open access article distributed under the terms and conditions of the Creative Commons Attribution (CC BY) license (<https://creativecommons.org/licenses/by/4.0/>).

1. Introduction

Ceramics and ceramic-reinforced metal matrix composites (CMMCs)-based coatings exhibit enhanced properties, including wear resistance, modulus and strength, chemical inertness, and properties at high operating temperatures [1–4]. Owing to these benefits, these coatings have been widely used in extreme working conditions, such as high load, wear, and temperature [5,6]. There are several commercialized applications of the aforementioned coatings in biomedical [7,8], aerospace [9], electronic [10], and other high-end engineering [11–13].

Because of the high hardness and elevated melting point, ceramics and CMMCs-based coatings are too difficult to process by conventional manufacturing processes [14–17]. A study [15] was conducted on diamond grinding of hot pressed Si₃N₄ and Al₂O₃, slip casted ZrO₂, and sintered SiC ceramics. It was found that hot-pressing, slip casting and sintering processes resulted in high cost and energy utilizations, while microcracks were observed due to grinding process. Recently, additive manufacturing (AM) has gained great attention and is still under continuous investigations in the case of ceramics and ceramic-reinforced MMCs-based coatings [18]. AM, as defined by the American Society for Testing and Materials (ASTM), is “a technique, opposite to the subtractive manufacturing

processes, of joining materials to make a 3D object using a CAD model, generally layer upon layer” [19]. In comparison to conventional coating processes, AM can produce coatings with reduced lead time, exemption from assembly or molds preparations, and less energy consumption [20–22].

1.1. Various Additive Manufacturing Processes

Based on the literature survey, AM process can be classified into two methods: (a) indirect and (b) direct. Indirect AM methods include fused deposition modeling [23], stereolithography [24], direct inkjet printing [25,26], layer-wise slurry deposition [27,28], and laminated object manufacturing process [29]. Generally, in indirect AM process, the coatings are produced using binding materials. Subsequently, the printed coating is sintered to eliminate the binding materials. Direct AM methods contain selective laser sintering [30,31], selective laser melting [32,33], and laser-melting deposition process [34,35]. The latter basically integrates the forming and densification procedures, producing a coating without the post-sintering requirement. Consequently, the coatings by direct AM method exhibit relatively higher density and purity, better mechanical characteristics, and require less time and energy, as compared to indirect AM method [36,37]. Furthermore, in direct AM methods, a laser beam is used as a heating source having high directionality and energy intensity, thus delivering a large amount of energy to the target (substrate) [38]. The direct AM method is also known as laser additive manufacturing (LAM) processes.

1.2. Laser Additive Manufacturing (LAM) Processes: Selective Laser Sintering and Melting

A schematic illustration of selective laser sintering (SLS) and melting (SLM) is presented in Figure 1. The only difference between SLS and SLM is that SLS involves the partial melting of powders, while the complete melting of powder debits is involved in SLM process. As a consequence, the deposited coatings via SLS yield low density and poor mechanical properties. On the other hand, SLM can produce near fully dense coatings with better mechanical properties [39]. Figure 1 shows that, at first, the substrate is moved downward by a mounted piston, leaving one layer-thickness space. Following on, a powder distributor spreads a specific amount of powder, evenly. The laser beam, which is controlled and directed by XY scanning mirrors and an $f-\theta$ lens, melts the powder and forms the first layer. Afterwards, the substrate moves downward to another layer thickness for the formation of the next layer. The designed component is fabricated by repeating the aforementioned steps [40].

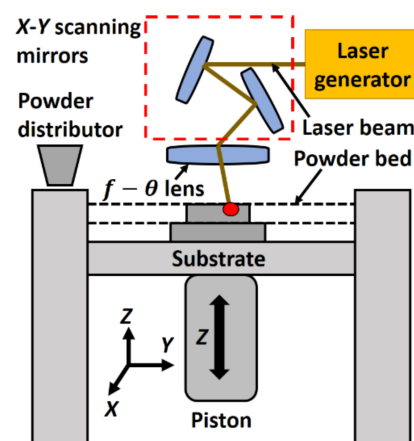


Figure 1. Schematic diagram of selective laser sintering and melting.

1.3. Laser Additive Manufacturing (LAM) Process: Laser Melting Deposition (LMD)

Figure 2 presents the schematic of the LMD process. Primarily, the substrate is melted by heat from laser radiation, generating a melt pool that captures and melts the powder provided by a powder nozzle. The powder particles are carried and mixed by a jet of gases,

such as argon and helium. As the laser source departs, the molten pool solidifies as a result of heat dissipation. The deposition head moves along the designated path, provided by a 3D CAD file, resulting in a layer deposition on the substrate. Afterwards, the deposition head moves upward by one-layer thickness for the deposition of the next coating. The previously deposited layer is partially melted, serving as a substrate for the formation of the next one. The aforementioned steps are repeated several times, until the designed 3D component is built layer after layer [37]. The LMD process mainly comprises laser engineered net shaping (LENS) and direct metal deposition (DMD) processes.

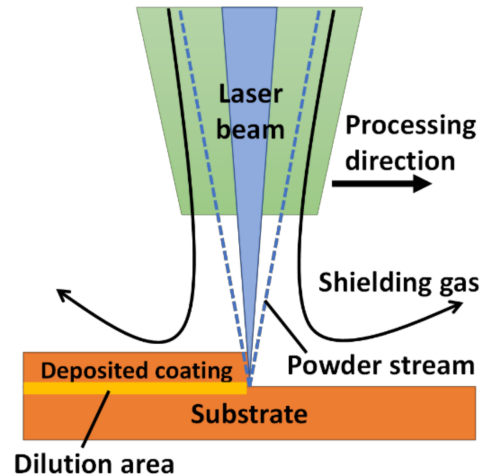


Figure 2. Schematic of laser melting deposition (LMD) process.

Among the developed LAM techniques, LMD has been widely used efficiently for the coating of a surface with a layer of ceramics and/or CMMCs. This process is usually carried out on the surfaces of bulk (new/worn-out) materials with the emphasis on enhancing the surface characteristics or obtaining the desired biological, frictional, or chemical characteristics for a given material [18]. Equipped with high energy density laser beams, LMD setups have demonstrated their capabilities to process materials with high hardness and elevated melting points. In comparison to SLS and SLM processes, LMD procedure presents the advantages of low effort intensity and high fabrication efficiency [41–43]. Besides the benefits mentioned above, difficulties such as poor bonding, cracking, or lower toughness exist, however, in ceramics and CMMCs-based coatings [44]. The solutions to these issues require major dedication from scientists and researchers. The possible solutions include process optimization, adding a buffer layer and/or functionally gradient composite (FGC) layers, integrating the ultrasonic vibration, pre/post-substrate heating, adding additive materials, and tailoring the novel microstructure [45–49]. This review paper compiles the developments in the LMD based coatings of ceramics and CMMCs. Further, the properties of such coatings, existing main issues, and their solutions are discussed.

2. Methodology

A review of literature 2000–2021 was carried out using Scopus and other databases, focusing on the keywords “selective melting/sintering” and “laser-melting deposition”. Special care was paid to originality and elimination of any repetition, incomplete, or hardly accessible (language) reports. The articles were screened for ceramic and ceramic-reinforced metal matrix composites coated by LMD only. The results were evaluated and compiled in the review. A scheme of applied procedure is available in Figure 3.

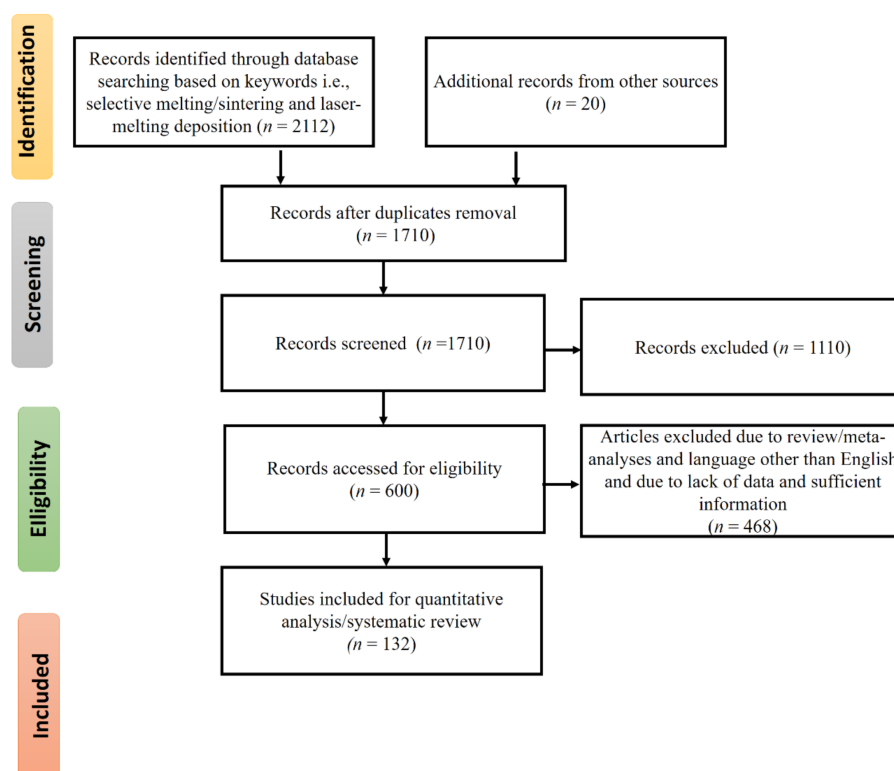


Figure 3. Review content according to PRISMA guidelines.

3. Coatings by LMD

There are two major types of near-net shape LMD coatings identified through the literature survey: (a) ceramics and (b) CMMCs-based coatings.

3.1. Ceramics-Based Coatings: Compositions and Properties

The LMD process has the capability to process ceramics having high hardness and a melting point up to 3000 °C. The following coatings have been identified based on the literature survey.

3.1.1. Alumina-Based Coatings

Alumina (Al_2O_3) is a white or nearly colorless crystalline substance that is used as a preliminary material for the smelting of aluminum metal. It also serves as a raw material for a broad range of advanced ceramic products and as an active agent in chemical processing [50]. The properties of pure alumina are given in Table 1.

Table 1. Properties of alumina [51].

Composition	$\text{Al}_2\text{O}_3 + \text{MgO}$	
Properties (Units)	Porosity (%)	<0.10
	Purity (%)	99.9
	Density (g/cm^3)	3.0–4.0
	Young's modulus (GPa)	350–380
	Bending strength (MPa)	7500
	Poisson's ratio	0.23
	Hardness (HV 0.1)	2100–2200
	Coefficient of thermal expansion ($\times 10^{-6}/\text{K}$)	8.0

Various studies have been carried on the coatings of Al_2O_3 . Recently, fully dense bulk Al_2O_3 structures were deposited via LMD with a 0.5 kW continuous wave Nd: YAG laser on a 3-mm-thick Al_2O_3 substrate. It was found that the deposited layers show anisotropy

in mechanical properties with a high compressive strength perpendicular to the build direction and columnar grains parallel to the deposition direction. Heat treatment did not change the strength and anisotropy, but the grain size increased from 6 to 200 nm. In addition, the hardness increased from 1550 to 1700 HV [35]. In another study, the effects of input deposition variables, including laser power, deposition head scanning speed, and powder feeding rate on deposition quality were analyzed. The laser power improves the length, width, surface roughness, flatness, powder efficiency, and microhardness of the deposited clad, but an inverse relation has been found between laser power and clad height. An increment in laser scanning speed causes a decrease in length, width, height, powder efficiency, surface roughness, and microhardness, but with a positive impact on flatness. However, a random behavior was found with regard to the powder feeding rate [36].

Pure alumina coatings (black/white) were deposited by LENS on Ti6Al4V substrates [52]. The coatings showed many evenly distributed surface cracks. The formation process effects both the volatility degree of oxide impurities in the particles, as well as the chemical elements and phase compositions in the samples. The development of the second phase is a major source for obtaining the black coatings and promoting the formation and propagation of surface cracks in the coating. An analytical model was developed to avoid a huge number of experiments for finding the optimal deposition parameters. The analytical formulae were presented, which could reveal the relationship between the operating parameters and physical properties of the Al_2O_3 parts to be fabricated [53].

The effects of laser scanning speed on the typical defects, microstructure, and mechanical properties of prepared samples were investigated, resulting in optimized process parameters [54]. The results showed that the laser scanning speed has a substantial influence on the macroscopic defects, microstructure characteristics, and mechanical properties. Slow laser scanning speed resulted in longer retaining time of the molten pool, which was beneficial to pore suppression. A fast scanning reduced the temperature gradient at the bottom of the melt pool to achieve crack-free depositions. The fracture toughness of the coatings gradually increased as the scanning speed increased, while a parabolic behavior was observed in the case of flexural strength. The optimal deposition was achieved at a scanning speed of 300–500 mm/m. The deposited material had up to 98% densification at this scanning speed, resulting in 1640 HV hardness, $3.75 \text{ MPa} \cdot \text{m}^{1/2}$ fracture toughness, and 212 MPa flexural strength. Figure 4 shows the SEM images of the typical microstructure of alumina + aluminum titanate composite ceramics. All samples contain dark and bright phases. The dark $\alpha\text{-Al}_2\text{O}_3$ phase accounts for the main volume fraction, while the $\text{Al}_6\text{Ti}_2\text{O}_{13}$ one is distributed in a network. For low and medium scanning speeds (Figure 4a–d), the Al_2O_3 grains' length along the deposition height is slightly longer than that perpendicular to the deposition direction. When using high-scanning speeds (Figure 4e,f), the preferential growth of Al_2O_3 grains along the deposition direction is significantly weakened.

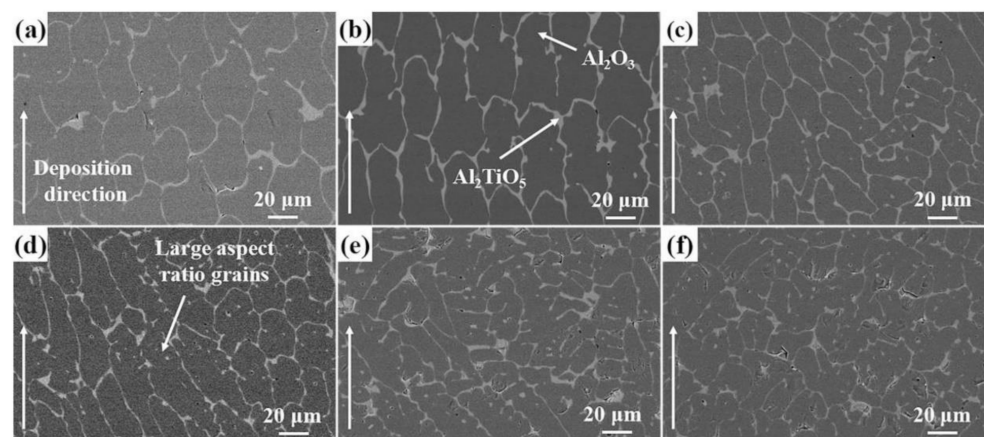


Figure 4. Microstructure of alumina + aluminum titanate composite ceramics for a scanning speed of 50 (a), 100 (b), 300 (c), 500 (d), 700 (e), and 900 (f) mm/min [54]; with permission from Elsevier.

3.1.2. Hydroxyapatite-Based Coatings

Hydroxyapatite (HAP) materials have gained interest from researchers because of outstanding biocompatibility, osteoconductive characteristics, and similarity to the inorganic component of human bones. They are widely used in biomedical materials [55,56], bone tissue engineering scaffolds [57], bioactive coatings [58], soft tissue repairs [59–62], drug delivery systems [63–68], and column chromatography for rapid fractionation of biomolecules [69,70]. HAP materials are also probable aspirants for usage in cell targeting, fluorescence labeling, and imaging and diagnosis materials [71,72]. The properties of HAP are given in Table 2 [73].

Table 2. Properties of hydroxyapatite [73].

Formula	$\text{Ca}_5(\text{PO}_4)_3(\text{OH})$
Composition	Ca + P
Theoretical density	3.156 (g/cm^3)
Hardness	500–800 (HV)
Tensile strength	40–100 (MPa)
Bend strength	20–80 (MPa)
Compressive strength	100–900 (MPa)
Fracture toughness	1.0 ($\text{MPa}\cdot\text{m}^{1/2}$)
Young's modulus	70–120 (GPa)

HAP was coated on Ti6Al4V using the LMD process [74]. One can obtain coatings with decent metallurgical bonding and slight dilution. The microstructural and mechanical properties, chemical composition, and bio-activities of the produced coatings were studied. The results showed that the laser power has a great impact on microstructure evolution, mechanical characteristics, and retainment of HAP coatings. Laser power equivalent to 750 W yielded no dilution. The microhardness results (1100 HV) inferred a strong intermetallic–ceramic bonding, which means that the coating at 750 W can last a long time during service. The hardness increases from the top to the bottom of the coatings or near to the heat-affected zone. The soak tests revealed that the surface of the coating had un-melted HAP crystals. Figure 5 shows the SEM images of the HAP coatings.

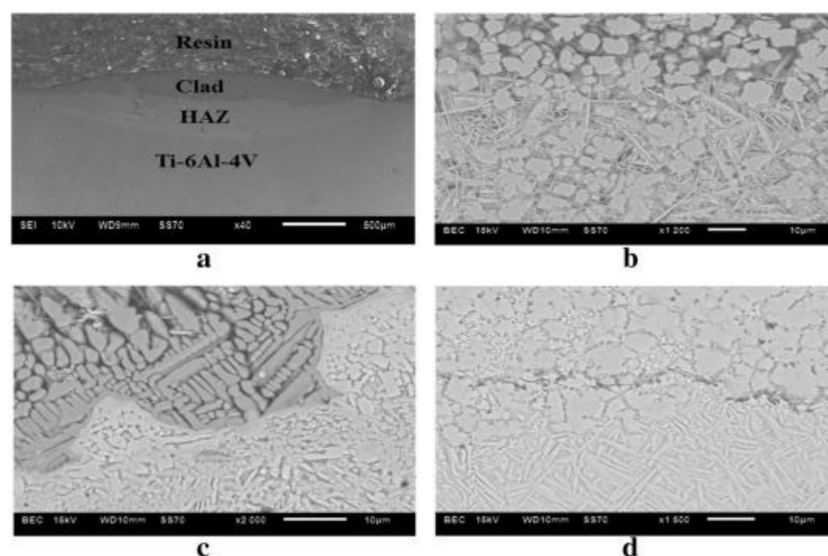


Figure 5. SEM images of hydroxyapatite (HAP) coatings after etching at 750 W (a), cross-section (b), cross-section clad and heat-affected zone (c), and cross-section heat-affected zone and Ti6Al4V substrate (d) [74]; published under open-access license by Elsevier.

HAP + yttria-stabilized zirconia (YZS) composite coatings were cladded by LMD on a titanium alloy substrate. The effects of zirconia on the microstructure, mechanical

properties, and the formation of tricalcium phosphate from the HAP + YSZ composite coatings were evaluated. The experimental results showed that adding YSZ in coatings was favorable to the composition and stability of HAP, which leads to the improvement of adhesion strength, microhardness, and micro-toughness [75]. Two types of porous HAP coatings were produced and tested with regard to their reprecipitation in a semi dynamic simulated physiological solution. Coatings having higher porosity were produced using a 355 nm laser wavelength, exhibited substantial reprecipitation more quickly than those deposited by a 266 nm laser wavelength. The dissolution of the non-HAP phases played a key role in the reprecipitation of HAP-like material. The Ca/P ratio of the coatings became nearer to the hypothetical value of HAP. The reprecipitation resulted in a very condensed morphology, suggesting a mechanically robust structure after reprecipitation. Despite dissolution and reprecipitation, the coatings showed sufficient stability in the solution and no significant loss of the coatings were found. Such results prove that HAP coatings can be used in clinical applications [76].

HAP coatings were deposited onto mild steel substrates under several laser power and stand-off distance conditions. The results indicated that microhardness and deposition efficiency increased with increasing power and stand-off distance. Porosity and surface roughness decreased as the Ca/P ratio steadily decreased [77], as shown in Figure 6.

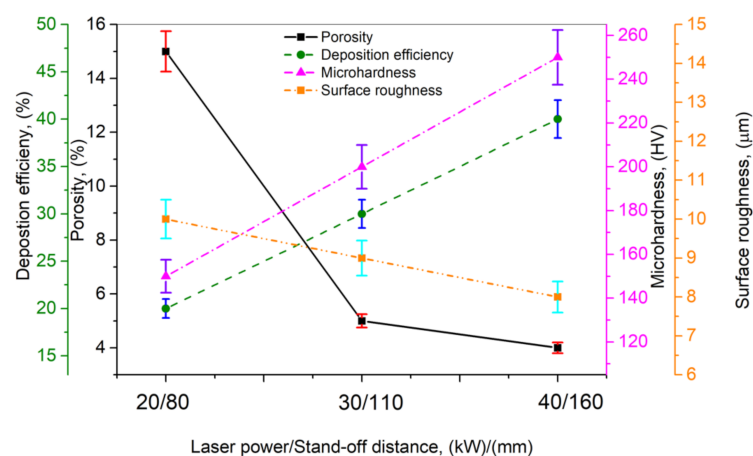


Figure 6. Effect of laser power/standoff distance on porosity, deposition efficiency, microhardness, and surface roughness; based on the data given in Reprinted from permission from [77]. Copyright year Copyright owner's name [77].

3.1.3. Zirconia-Based Coatings

Zirconium dioxide (ZrO_2), also known as zirconia, is a white crystalline oxide of zirconium. The most natural form of ZrO_2 , with a monoclinic crystalline structure, is the mineral baddeleyite [78]. The properties of pure zirconia are given in Table 3.

Table 3. Properties of pure zirconia [51].

Properties (Units)	Zirconia
Chemical composition	$\text{ZrO}_2 + \text{Y}_2\text{O}_3 + \text{MgO}$
Porosity (%)	<0.10
Purity (%)	95.0–97.0
Density (g/cm^3)	5.0–6.0
Young's modulus (GPa)	200–220
Bending strength (MPa)	500–1000
Poisson's ratio	0.30
Hardness (HV 0.1)	1200–1250
Coefficient of thermal expansion ($\times 10^{-6}/\text{k}$)	11.0

ZrO_2 (95 vol.%) + Al_2O_3 (5.0 vol.%) present improved toughness, outstanding corrosion and thermal resistances, decent biocompatibility, and reasonable mechanical properties via altering ZrO_2 content and powder preparation parameters [79–81]. It is widely used in several commercial applications, including orthopedic parts [79], dentistry [82], valve seats and tubes [80], manufacturing tools [12], and bearing parts [11]. An Al_2O_3 15-mm-thick plate was coated with a mixture of ZrO_2 and Al_2O_3 (without any binding material) via the LMD process, with a eutectic ratio of 41.5 and 58.5 (wt.%), respectively. The average microhardness of the deposited Al_2O_3 + ZrO_2 eutectic ceramic was 17.15 GPa, and the fracture toughness was $4.79 \text{ MPa}\cdot\text{m}^{1/2}$. In addition, as a consequence of rapid melting/solidification, the microstructure (fine-grained) with an eutectic spacing of 100 nm was achieved [1]. Figure 7 shows the microstructure of the deposited coating, which is comprised of light and dark phases. The tetragonal light phase is ZrO_2 , while the dark one is Al_2O_3 . The two phases contain a columnar colony microstructure of faceted alumina grains growing along the (0 0 0 1) sapphire *c*-axis. The lamellar microstructure is the primary element of the Al_2O_3 + ZrO_2 eutectic ceramic, and a key aspect in defining the mechanical properties of the specimens.

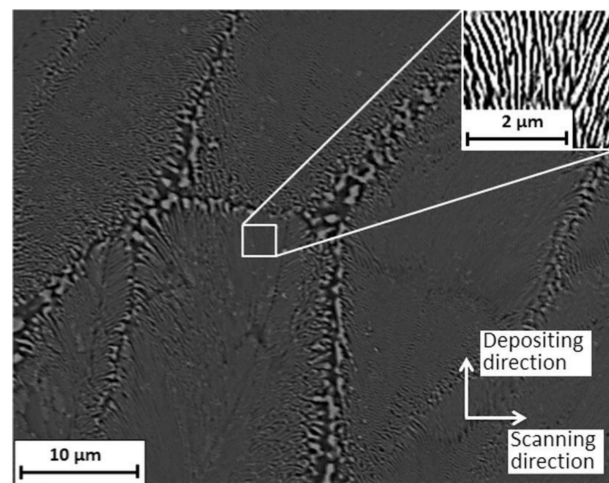


Figure 7. Microstructure of the deposited alumina + zirconium dioxide ceramic [1]; with permission from Elsevier.

These microstructures were further refined and uniformized, equivalent to 60.29 nm eutectic spacing, by integrating an ultrasonic vibration in the LMD process [83].

The integration of ultrasonic vibration with the LMD step-up plays a significant role in improving the mechanical properties and microstructure of the deposited coatings. In this context, ZrO_2 (10 wt.%) and Al_2O_3 (90 wt.%) coatings were deposited on a titanium substrate [2]. Figure 8 shows the effects of ultrasonic vibrations. It was found that the hardness (1670–1760 HV) and stress-bearing capacity (280–450 MPa) of the deposited coatings are improved, while the wear rate decreased (20×10^{-5} – $8 \times 10^{-5} \text{ mm}^3/\text{Nm}$) significantly. This can be attributed to the fact that with the integration of ultrasonic vibrations in the LMD process, the grain refinement and homogenized material dispersion occur, thus improving the properties of deposited materials.

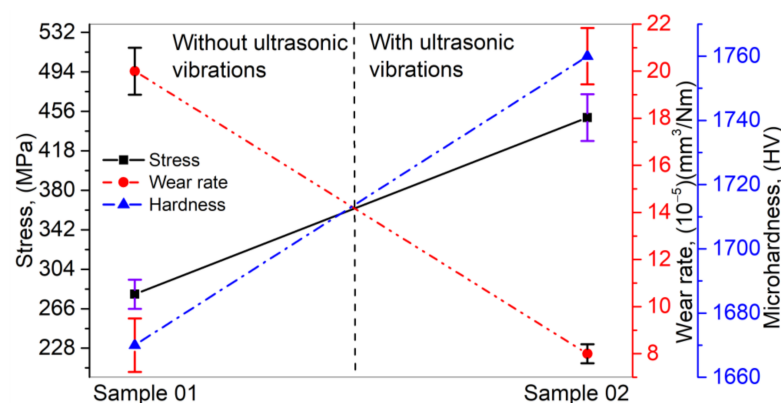


Figure 8. Stress, wear rate, and microhardness of the deposited $\text{ZrO}_2 + \text{Al}_2\text{O}_3$ coatings on titanium substrate: with and without ultrasonic vibrations; based on the data from [2].

LMD has been proposed and utilized to fabricate customized zirconia-toughened alumina (ZTA) coatings in a shorter cycle time at a lower cost. Investigations have been reported on the effects of laser power on ZTA depositions with regard to microstructures and mechanical properties. Experimental results exhibit that at lower levels of zirconia contents (5, 10 and 20 wt.%), a novel three-dimensional quasi-continuous network (3DQCN) microstructure is tailored. In contrast, for higher zirconia contents (30, 35 and 41.5 wt.%), the eutectic microstructure dominates the whole deposition. Both microstructures are, however, beneficial for toughening the ZTA coatings. Moreover, the 3DQCN microstructure contributes to the hardening of ZTA depositions [84].

3.1.4. Silicon Carbide-Based Coatings

Silicon carbide (SiC) is a solid mineral crystal, which is used as a semiconductor and a ceramic, commonly referred to as carborundum. It appears as colorless and transparent crystals. When impurities are added, SiC crystals change to green or blue depending on the level of impurity. SiC possesses excellent hardness and strength, which makes it a potential candidate for the manufacturing of fast, high-voltage and high-temperature devices [85]. SiC properties are given in Table 4 [85,86].

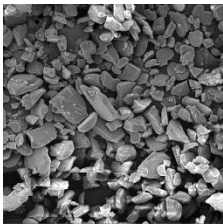
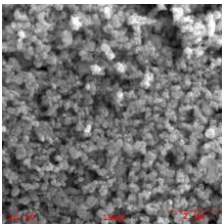
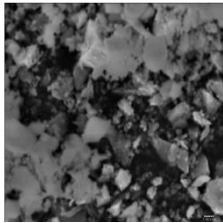
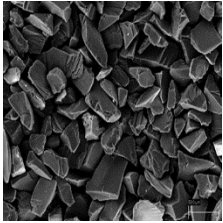
Table 4. Properties of silicon carbide [85,86].

Properties (Units)	Silicon Carbide
Chemical composition	SiC + FC + Fe_2O_3
Max. service temperature ($^{\circ}\text{C}$)	1380
Density (g/cm^3)	3.02
Bending strength (MPa)	280 (1200°C)
Elastic modulus (GPa)	300 (1200°C)
Thermal conductivity (W/mk)	45 (1200°C)
Thermal expansion coefficient ($\times 10^{-6}/\text{k}$)	4.5
Mohs hardness	13

There are several studies carried out on the coatings of SiC using the LMD technique. A detailed investigation has been carried out on the optimization of the SiC laser coating on titanium alloy. The microstructure, phase composition, and microhardness of the coatings were studied. Crack-free coatings with a significant increase in hardness from 245.5 to 1923.5 HV were obtained [87]. In another study, an attempt was made to coat a compositionally graded SiC dispersed phase on the surface of mild steel substrate by the LMD technique. A continuous wave CO_2 laser was used, with the simultaneous feeding of SiC particulates, assisted by argon gas. Within the coatings, SiC particles were found to be partially dissociated, with a higher degree of dissociation at the bottom as compared to the top area. The microhardness of the surface was improved from the 190 to 600 HV, and

decreased gradually from the top to the bottom of the coating. The cumulative depth of wear also decreased from 16 to 3 μm [88]. Silicon infiltrated silicon carbide (substrate) was coated with SiC + SiO₂ and SiC + Si particles by LMD. An Nd: YAG laser source delivering an average power of 920 W (pulse rate = 10 Hz, pulse width = 1 ms) was used to apply such coatings using the powder blowing technique. The results demonstrated that the use of the SiC + SiO₂ powder mixture produces a severe damage of the substrate, whereas the use of the SiC + Si mixture leads to the formation of sound coatings without substrate damage [89]. Table 5 summarizes the morphologies of the ceramic powder mentioned above.

Table 5. Various ceramic powders and their morphologies.

Powder Type	Manufacturer	Particle Size	Images	References
Alumina	VAW aluminium AG	3–6 (μm)		[35]
Hydroxyapatite	Sigma Aldrich	20 (nm)		[57]
Zirconia	Fanmeiya Advanced Materials	0.16–0.60 (μm)		[78]
Silicon carbide	Leading Manufacturer	50–75 (μm)		[85]

3.1.5. Applications of Ceramic-Based Coatings: Wear, Biomedical, and Chemical

Ceramic coatings have been proved to enhance wear resistance of a given material. CaF₂ + Al₂O₃ ceramics' coatings were deposited on an Al₂O₃ substrate by the LMD process [90]. Scanning electron microscope analyses showed that the CaF₂ particles were homogeneously dispersed in the matrix of Al₂O₃. CaF₂ presented a noticeably low friction coefficient, resulting in significantly improved self-lubricating and wear resistant coatings.

Biomedical industries demand not only an enhanced wear resistance but also biocompatibility. Si₃N₄ + tricalcium phosphate (TCP) bio-ceramic coatings were deposited on a Ti6Al4V substrate [91]. Within the coatings, Si₃N₄ was found to be non-cytotoxic and can protect the Ti6Al4V substrate from wear and tear. In addition, the bioresorbability of TCP enabled fast bone development and contributed to its incorporation with the bone tissue [92].

Ceramics are also characterized by excellent chemical stability. To protect heat exchanger tubes from fireside erosion and corrosion, a coating of WC + Co on a low carbon steel substrate was carried out by the LMD process [93]. Results indicate that the deposited coatings gave excellent hardness and adequate wear resistance in comparison to pure material (low carbon steel substrate).

The rise in the abrasive resistance could be due to the WC + Co addition and explains also the increase in the coefficient of friction, and therefore the decrease in the wear volume. It, in return, increases the hardness value. These results are illustrated in Figure 9.

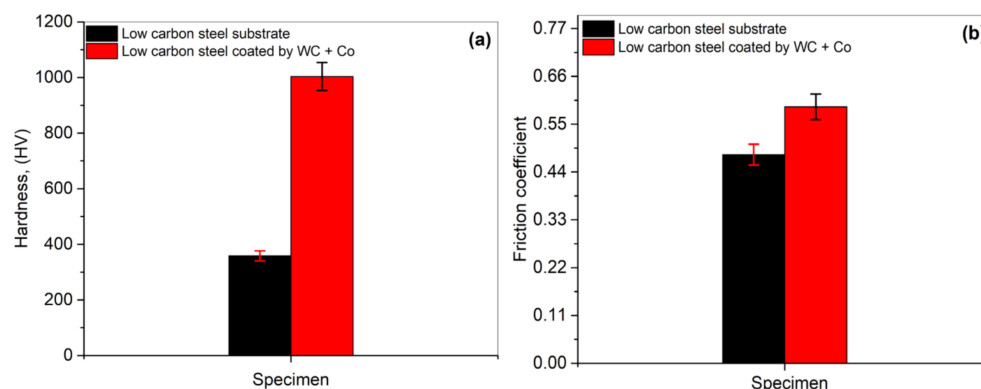


Figure 9. Comparison of the (a) hardness and (b) friction coefficient, with and without coatings; based on the data from [93].

3.2. Ceramics Reinforced Metal Matrix Composites (CMMCs)-Based Coatings: Compositions and Properties

Ceramic reinforced metal matrix composites (CMMCs) are usually composed of two types of materials: (a) ceramics + non-metals and (b) ceramics + metal/metal alloys. However, in the LMD process, option (b) is commonly used. For deposition, they are premixed or mixed coaxially using powder feeders. Through literature survey three types of CMMCs have been identified: (a) nickel-based, (b) Inconel and invar-based, and (c) titanium-based.

3.2.1. Nickel-Based CMMCs

Nickel (Ni) matrices reinforced by ceramics (NCMMCs) are promising materials with a vast range of applications, including aerospace, chemical, and petrochemical industries [94]. They present high corrosion, fatigue, and wear resistances, as well as high hardness due to ceramic reinforcement. Titanium carbide (TiC) reinforced NCMMCs were coated on a Ni substrate via LMD [95]. The NCMMCs exhibited a high microhardness value of 370 HV in comparison to 165 HV for pure Ni. The high-volume fraction of TiC is reflected in the higher microhardness. In addition, tribo-studies were carried out for both compositions. From Figure 10, it is clear that the TiC phases were beneficial in reducing the friction coefficient (~ 0.20) in comparison to the pure Ni sample (~ 0.75).

Ni + Ti + C coatings were deposited on low carbon steel by the LMD process [96]. A total of three compositions, including 20, 40 and 60 (vol.%), were deposited. The influence of TiC vol.% on phase transformation, microstructure evolution, hardness, and wear resistance was analyzed. The analyses exhibited that the composites consisted of TiC + Ni phases. TiC particulate size increased from 3 to 10 μm , when the TiC (vol.%) was increased from 20% to 60%. In addition, the hardness was improved from 365.6 to 1897.6 HV, while the value of wear resistance changed from 20 to 6×10^{-3} g. Figure 11a–c are SEM images of Ni + TiC cross-sections. When the TiC volume fraction is 20 vol.%, the size of the in situ forming TiC particles is smaller, and the average size is less than 3 μm . If the TiC volume fraction in the Ni-Ti-C system is 60 vol.%, one clearly observes that the in situ fabricated TiC particles are spherical and bigger, with an average size of about 10 μm .

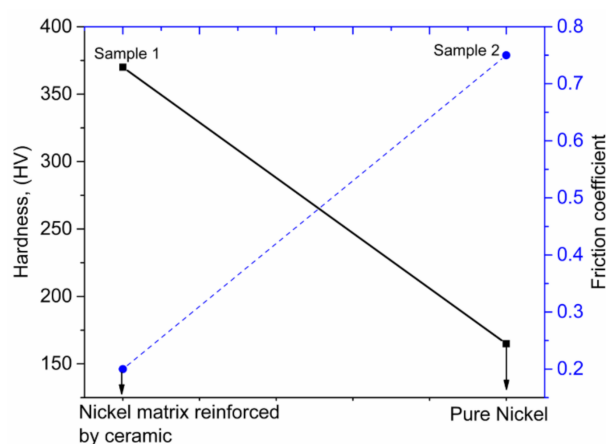


Figure 10. Hardness and friction coefficient of Nickel (Ni) matrix reinforced by ceramics (NCMMCs); based on the data from [95].

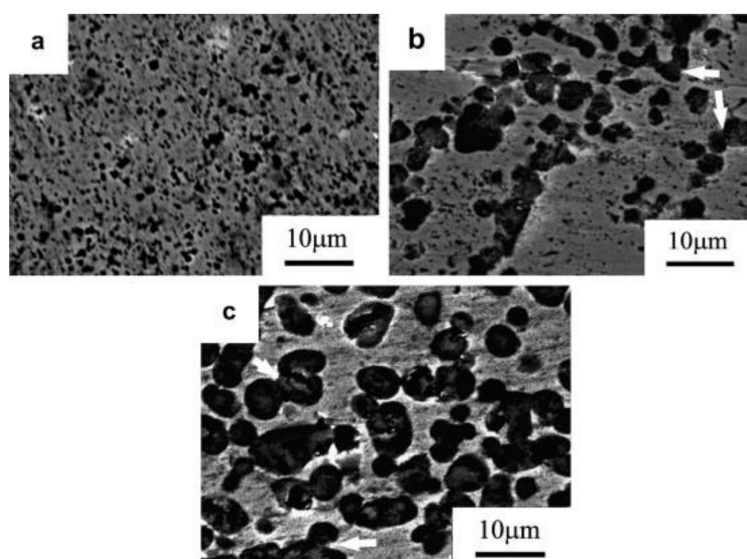


Figure 11. SEM images of Ni + Ti + C microstructures by LMD: 20 (a), 40 (b), and 60 (c) vol.% TiC [96]; with permission from Elsevier.

3.2.2. Inconel and Invar-Based CMMCs

Recently, Inconel and invar-based CMMCs have been explored with regard to their applicability in different industries. For this purpose, the effects of laser energy input per unit length (LEIPUL) on microstructure and mechanical characteristics were analyzed in the case of TiC-reinforced Inconel 625 coated on a C45 carbon steel substrate [97]. The results show that high energy input led to an efficient Marangoni convection within the molten pool, resulting in a refined (from 34.1 to 27.2 μm) and homogenized dispersion of TiC reinforcements. A proper increase in the applied LEIPUL to 100 kJ/m led to a considerably low average friction coefficient of 0.30 and reduced wear rate of $1.3 \times 10^{-4} \text{ mm}^3/\text{N m}$ for the LMD-processed coatings. These values are explained by the formation of the adherent and strain-hardened tribo-layer on the worn surface during sliding wear tests. The formation of the refined columnar dendrites of the Ni–Cr γ matrix combined with the homogeneously distributed ultra-fine reinforcing particles and contributed to the enhancement of wear performance. The significant coarsening of columnar dendrites of the matrix at an excessive LEIPUL of 160 kJ/m lowered the tribological property. These results are shown in Figure 12.

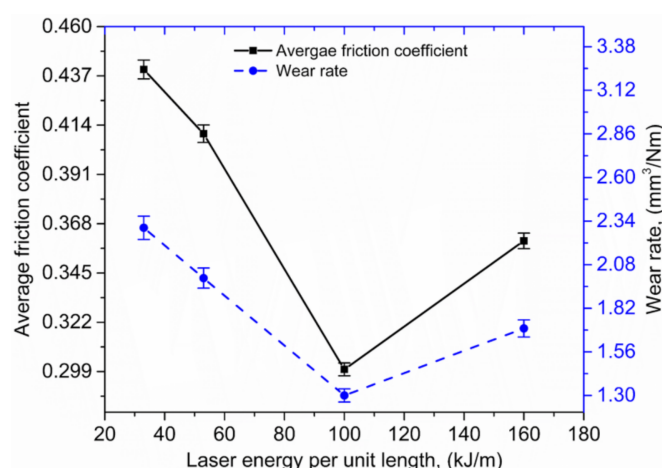


Figure 12. Friction coefficient and wear rate of TiC-reinforced Inconel 625 coated on a C45 carbon steel substrate; based on the data from [97].

The rapid heating and solidification involved in the LMD process generate a high temperature gradient and thermal stress within the fabricated parts. This introduces defects, including cracks, warpage, and delamination. Invar has been proved beneficial to decrease the coefficient of thermal expansion (CTE). Invar is basically a combination of 64 wt.% Fe + 36 wt.% Ni. TiC-reinforced Invar coatings were manufactured via the LMD process [98]. Experimental results, in Figure 13, show that composites showed high hardness, yield strength, and thermal expansion coefficient, while elongation decreased exponentially. This can be explained by noting that the interfacial bonding between the matrix and reinforcement is mandatory to achieve better elongation. A weak adhesion between the two phases restricts the load transfer from the matrix to reinforcement, thus inducing a declination of elongation.

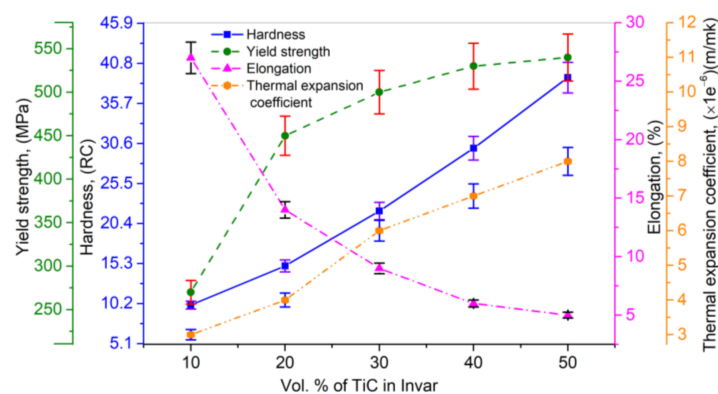


Figure 13. Effect of vol.% of TiC in invar: hardness, yield strength, elongation, and thermal expansion coefficient; based on the data from [97].

3.2.3. Titanium-Based CMMCs

Ceramic reinforced titanium (Ti) matrix composites (TCMMCs) have been widely used in aeronautical and biomedical industries due to their high strength-to-weight ratio and exceptional biocompatibility. TiC [99,100], TiN [33] and TiB [3] are identified as most commonly used reinforcements for titanium matrices. TiC-reinforced TCMMCs were coated on TA15 substrate via LMD process and the effects of TiC content on microstructure and tensile properties were studied [99]. TMC with 5 vol.% TiC exhibited better ultimate tensile strength (UTS) but worse ductility in comparison to titanium alloys. While increasing the TiC from 5 to 15 vol.%, both UTS and ductility of TCMMCs depreciated dramatically. These results are shown in Figure 14.

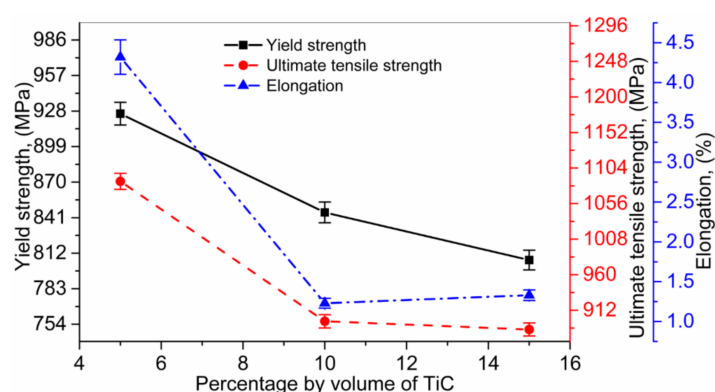


Figure 14. Effect of vol.% of TiC on: yield strength, ultimate tensile strength, and elongation; based on the data from [99].

Among all types of ceramic materials, TiB is considered one of the most suitable for reinforcement [34] for the following reasons: (i) small quantity of TiB hugely improves the mechanical properties of TCMMCs, (ii) thermal stress at the interfaces of TiB + Ti are diminished due to their similar densities and CTEs, (iii) TiB is a steady phase and no intermediate phase occurs between TiB and Ti, and (iv) a strong metallurgical bonding occurs between TiB and Ti [101]. TiC + Ti6Al4V TCMMCs were produced with 10, 20 and 30 vol.% reinforcing ceramic. The analysis revealed the presence of partially melted TiC particles embedded in the Ti matrix, along with fine dendrites of re-solidified ceramic. The dendritic structures in the Ti-based composites were confirmed as TiC. TCMMCs showed an increase in microhardness with increasing ceramic (carbide) content, reaching a peak of 550 HV in the Ti-based TCMMCs [102]. These results are presented in Figure 15.

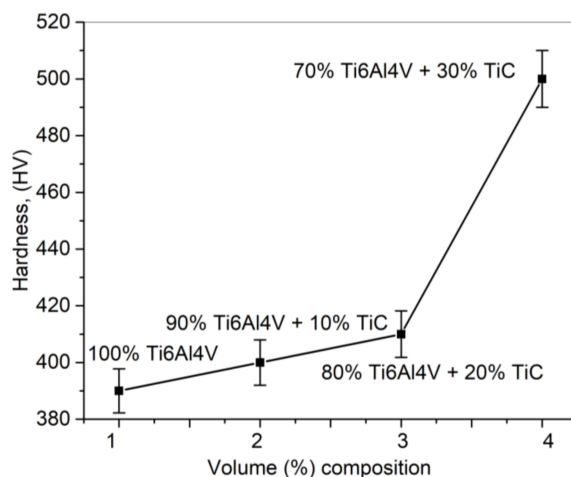


Figure 15. Effect of vol.% of TiC on hardness; based on the data from [102].

3.2.4. Applications of Ceramics Reinforced Metal Matrix Composites (CMMCs)-Based Coatings: Wear, Biomedical, Chemical, and Electrochemical

One of the common issues of ceramic coatings is the delamination which occurred between the substrate and coatings. Delamination usually occurs due to poor bonding between the substrate and coating to be deposited. Recently, CMMCs have gained the interest of researchers and scientists as they have proved beneficial in solving the aforementioned issue. In CMMCs, hard ceramic reinforcements in the matrix act as load-bearing elements, which can restrain plastic deformation and prevent matrix material from wear and tear. It makes them a potential candidate for wear and load-bearing applications. In situ TiB + TiN-reinforced TCMMCs were deposited on a Ti substrate by the LMD process using a premixed Boron nitride and Ti6Al4V powder particulates [103]. The fine dispersion of TiB

and TiN reinforcements within the Ti matrix remarkably improved the wear resistance of the Ti substrate. Nickel-based matrix reinforced with WC + W₂C carbides were coated by a CO₂ laser via LMD on a low carbon steel substrate [104]. Different coatings were made with three different particle sizes of the carbides and volume fractions ranging from 0% to 50%. It was evidenced that an increase in vol.% WC + W₂C carbides and a decrease in carbide size favored the enhancement of hardness (from 200 to 350 HB) and wear resistance (200 times larger than without carbides). In addition, a small amount of carbides was sufficient to significantly improve wear resistance.

CMMCs have proved their capabilities for implants with minimized wear-induced osteolysis and aseptic loosening [105]. TCMMCs, including reinforced TiN [106] and SiC [107], possess high biocompatibility, thus, they are widely used on metallic substrates to improve the applicability of metallic substrates for biomedical applications. These coatings exhibited in vitro excellent cell–material interaction and no toxicity, proving their high potentiality for load-bearing implants, e.g., hip, knee, and shoulder.

Ni₂Si + NiSi composites were fabricated on a 0.2% carbon steel substrate by the LMD process [4]. The coatings established outstanding chemical and electrochemical corrosion resistance properties. Novel composite coatings, including TiC + Stellite-6, WC-reinforced cobalt matrix, MoSi₂-reinforced Stellite-6 matrix, and MoSi₂-reinforced steel matrix composites, were deposited on an AISI 1018 steel substrate to improve the slurry erosion wear rate [5]. The deposited coatings exhibited an enhanced erosion rate as compared to pure materials.

4. Modelling Approaches

One of the productive ways to understand the coating process by LMD is to simulate it before performing the actual experiment. Numerous studies have been conducted to classify the relation between process parameters and deposited coating. Acharya et al. [108] combined computational fluid dynamics and phase-field models to simulate grain formation based on the primary operating parameters, including laser power and scanning speed. Fergani et al. [109] presented a mathematical model to analyze the residual stress distribution within the coated layers, while Chen et al. [110] developed a finite element (FE) analysis model to examine melt-pool dimensions and the deposited layer profile. Yu et al. [111] developed a FE model to simulate residual stresses based on primary operating parameters. FE modelling is usually time consuming and requires a dedicated computing setup and specialized skills to generate a solution. Further, FE model solution accuracy depends on meshing accuracy: a fine mesh requires higher computation time.

To solve this mystery, various efforts have been carried out to develop time-efficient analytical models. Mahmood et al. [112] developed an analytical model to simulate the dimensions for all deposited layers and corresponding residual stresses. The model was able to provide an answer within an accuracy of 10–15% mean absolute deviations. In another study by Mahmood et al. [113], an analytical model was presented to simulate powder flow from a 3-jet powder nozzle and its interaction with a laser beam. This model was computationally efficient and was able to estimate results with an accuracy up to 10% mean absolute deviations. A model to estimate average grain size and mechanical properties, based on primary operating parameters, was presented [114]. This model was able to predict results with 8% mean absolute deviations. Various analytical models have been presented to estimate temperature distribution within deposited coating using non-Fourier and two-temperature model techniques [115–119]. These models can be used for process optimization by linking them with optimization software or an artificial neural network before performing actual experiments [120].

5. Coatings by LMD: Existing Difficulties, Solutions, and Future Trends

One of the major difficulties in coating ceramics over metallic substrates is the lack of bonding between the two, which can be described in terms of poor compatibility due to differences in thermal, mechanical, and physical properties [44]. Low wettability, defined

as the ability of liquid to preserve an interaction with a solid surface between the deposited coating and substrate, also accounts for such phenomenon, causing a metallurgical bonding failure [121]. Due to poor bonding, the coated layers will simply peel off from the substrate. There are several methods available to improve the bonding between the coated layers and substrate, compiled in Table 6, Figure 16.

Table 6. Different techniques to optimize the bonding between substrate and coatings.

Technique	Illustration	References
Integrating the ultrasonic technology with LMD process	With periodical positive–negative pressure, ultrasonic vibration produces two non-linear actions of acoustic streaming and transient cavitation. The absorption of acoustic oscillations in liquid materials generates a stable flow, also known as acoustic streaming. Transient cavitation assists the formation, growth, pulsation, and collapse of the micro-sized bubbles. These two non-linear actions facilitate material movement within the liquid, which is beneficial for regulating material dispersion. This in return reduces the thermal gradient, stresses, or cracks, and refines grain formation in the deposited coating.	[122–126]
Adding a buffer or functionally graded layer	Adding a buffer layer proved efficient for enhancing the compatibility between the deposited ceramic coatings and metallic substrate, thus rendering a firm bonding between them, as shown in Figure 16.	[47,48]

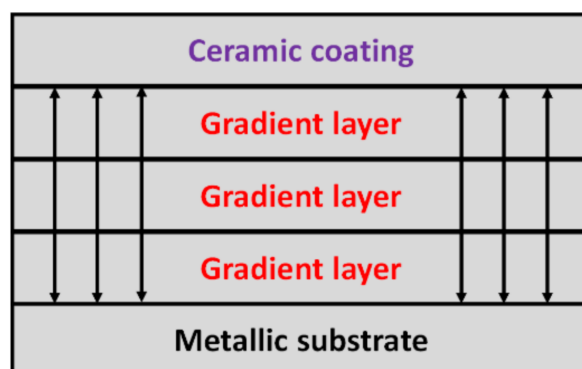


Figure 16. Inclusion of buffer or functionally graded material layer. This technique is commonly used in the medical industry.

Further, it is essential to optimize process parameters to melt down completely the material to be coated on the substrate and obtain an optimum bonding. In the LMD process, there are three primary operating parameters: laser power, scanning speed, and powder feeding rate. An optimum set of parameters is necessary to obtain well-balanced coating over a substrate [45,46]. This procedure is commonly known as “process optimization.” Due to rapid heating and cooling involved in the LMD process, cracks are usually induced due to a huge thermal gradient inherent to the LMD process [18]. The advent of cracks leads to poor mechanical properties and a shorter life span of the deposited coating. Moreover,

the presence of cracks can cause the failure of coating under cyclic loading [127]. It is therefore essential to eliminate cracks to fabricate fully dense coatings. This will ultimately improve the mechanical characteristics of the coated material. A few techniques have been compiled in Table 7.

Table 7. Different techniques to optimize the bonding between substrate and coatings.

Technique	Illustration	References
Addition of rare earth oxides	Rare earth oxides can change the dynamics of melt pool and are capable of preventing crack initiation and propagation via preventing dislocation movements.	[128]
Pre-/post-heating of substrate	The main purpose is to decrease the thermal gradient between the deposited coating and substrate. This process has been proved to successfully suppress the cracks in the LMD process. However, such treatments are time- and cost-consuming, requiring supplementary procedures and equipment. Further, this technique may even alter the required properties of the coated material.	[105,129]

As mentioned earlier, process optimization is an effective method to reduce crack formation; however, the process parameter window to manufacture crack-free parts is very tough to find. It may lead to large number of experimentations before finding an optimal set of parameters [53,130]. Despite reinforcing effects induced by the presence of rigid ceramic phases, CMMCs still exhibit severe issues resulting from reduced toughness and ductility [131]. A pressing problem that needs to be addressed is how to strengthen matrix materials without losing too much resilience and ductility. To avoid this, a three-dimensional quasi-continuous network (3DQCN) microstructure using TiB-reinforced TCMMCs was tailored using LMD process [64]. In 3DQCN, bright and dark regions were recognized as TiB reinforcement and Ti matrix, respectively. TiB was valuable for strengthening the composites, while Ti regions were able to increase the toughness and ductility of TCMMCs [132].

6. Conclusions

The investigation of ceramics and ceramic-reinforced metal matrix composites (CMMCs) by LMD has been explored and summarized herewith. The main conclusions are the following:

- Selective laser sintering (SLS), selective laser melting (SLM), and laser melting deposition (LMD) are commonly used laser additive manufacturing techniques. LMD has demonstrated capabilities to process materials with high hardness and elevated melting points due to the use of high intensity laser beams. In comparison to SLS and SLM, the LMD process presents the advantages of low work intensity and high fabrication efficiency.
- For LMD coatings, the proper selection of process parameters results in increasing the melting degree and in the uniformization of deposited coating properties. In addition, the side effects of high thermal stress and part distortion can be reduced or even eliminated by process optimization.
- LMD demonstrated viability to process ceramics and CMMCs. The coatings growing on surfaces of bulk materials improve their characteristics and bring biological and/or chemical attributes to the materials. Fabricated samples can be utilized in aerospace, biomedical, chemical, and electrochemical industries.

- In LMD, the good adherence of the deposited ceramics or CMMCs layers to the substrate is of great importance for obtaining high quality coatings. To achieve the desired adherence strength, one should optimize correspondingly the processing parameters. Whenever the process optimization fails, a buffer layer can be introduced in between coating and substrate, possibly in combination with ultrasonic vibrations.
- LMD CMMCs coatings exhibit remarkable features, including high strength at elevated temperatures, improved hardness, better fatigue resistance, and creep characteristics, which makes them appropriate for advanced technological applications. Opposite behavior of the elongation had been observed, while UTS and YS showed random behaviors. The interfacial bonding between the matrix and reinforcement is therefore mandatory to obtain better UTS and YS. The weak adhesion between phases limits the load transfer from matrix to reinforcement, thus decreasing UTS and YS. Consequently, a careful selection of reinforcement and their fraction (wt.%) in combination with the metal matrix is necessary to achieve optimum physical, thermal, and mechanical properties.
- In LMD, cracks are usually initiated by the large thermal gradient, resulting in coatings with weak mechanical properties and a short life span. Their number and size can be reduced by process optimization, pre-/post-heating of the substrate, additive materials, and/or the LMD integration with ultrasonic vibrations.
- In the case of CMMCs, LMD coating meets with major difficulties due to lowered toughness and ductility. These issues can be solved by tailoring suitable microstructures within the deposited coating.
- Any kind of post-processing would require special tools and high energy, thus increasing the fabrication cost, which limits the availability of CMMCs to niche applications. One should therefore identify the best balance between appropriate thermo-mechanical properties and low production cost in order to effectively promote the MMCs.
- New materials with improved properties could be fabricated by the optimum addition of matrix and reinforcement in powder form. Moreover, coatings with complex architecture such as multilayered structures or gradient composition can be easily obtained via in situ CMMCs. One should also explore the manufacturing of the precise composition of CMMCs using different laser sources by properly modifying the microstructure and mechanical, thermal, and electrical properties.
- LMD is expected to allow for sub-mm resolution and hence for an increased accuracy of the MMCs printed via LMD.
- The latest technique is to utilize an enhanced topology design. The coatings dimensions, restrictions, and the acting forces are specified in this case by the CAD/CAM user. The software calculates based upon the maximum resistance to stress and the most appropriate shape, in accordance with user requirements. The resulting shape is, however, in most cases unconventional and convoluted. 3D printing proved suitable to fabricate such coatings. LMD can further push forward the field by using CMMCs.

Author Contributions: Conceptualization, I.N.M.; methodology, M.A.M., C.R. and I.N.M.; software, M.A.M. and A.B.; validation, C.R., I.N.M. and N.B.; formal analysis, M.A.M. and A.B.; investigation, M.A.M. and A.B.; resources, C.R. and N.B.; writing—original draft preparation, M.A.M. and A.B.; writing—review and editing, C.R., I.N.M. and N.B.; supervision, C.R. and I.N.M.; project administration, C.R. and N.B.; funding acquisition, C.R. All authors have read and agreed to the published version of the manuscript.

Funding: This research and APC were funded by European Union's Horizon 2020 (H2020) research and innovation program under the Marie Skłodowska-Curie, Grant agreement No. 764935.

Institutional Review Board Statement: Not applicable.

Informed Consent Statement: Not applicable.

Acknowledgments: M.A.M. has received financial support from the European Union’s Horizon 2020 (H2020) research and innovation program under the Marie Skłodowska-Curie, grant agreement No. 764935. C.R. has received support by Romanian Ministry of Education and Research, under Romanian National Nucleu Program LAPLAS VI—contract no. 16N/2019. C.R., A.B., N.B. and I.N.M. acknowledge with thanks the partial support of this work under the POC-G Contract No. 135/2016.

Conflicts of Interest: The authors declare no conflict of interest.

References

1. Niu, F.; Wu, D.; Ma, G.; Wang, J.; Guo, M.; Zhang, B. Nanosized microstructure of Al_2O_3 - ZrO_2 (Y_2O_3) eutectics fabricated by laser engineered net shaping. *Scr. Mater.* **2015**, *95*, 39–41. [\[CrossRef\]](#)
2. Hu, Y.; Ning, F.; Cong, W.; Li, Y.; Wang, X.; Wang, H. Ultrasonic vibration-assisted laser engineering net shaping of ZrO_2 - Al_2O_3 bulk parts: Effects on crack suppression, microstructure, and mechanical properties. *Ceram. Int.* **2018**, *44*, 2752–2760. [\[CrossRef\]](#)
3. Hu, Y.; Cong, W.; Wang, X.; Li, Y.; Ning, F.; Wang, H. Laser deposition-additive manufacturing of TiB-Ti composites with novel three-dimensional quasi-continuous network microstructure: Effects on strengthening and toughening. *Compos. Part B Eng.* **2018**, *133*, 91–100. [\[CrossRef\]](#)
4. Wang, H.M.; Wang, C.M.; Cai, L.X. Wear and corrosion resistance of laser clad Ni_2Si /NiSi composite coatings. *Surf. Coatings Technol.* **2003**, *168*, 202–208. [\[CrossRef\]](#)
5. Tucker, T.R.; Clauer, A.H.; Wright, I.G.; Stropki, J.T. Laser-processed composite metal cladding for slurry erosion resistance. *Thin Solid Films* **1984**, *118*, 73–84. [\[CrossRef\]](#)
6. Man, H.C.; Zhang, S.; Cheng, F.T.; Guo, X. In situ formation of a TiN/Ti metal matrix composite gradient coating on NiTi by laser cladding and nitriding. *Surf. Coatings Technol.* **2006**, *200*, 4961–4966. [\[CrossRef\]](#)
7. Höland, W.; Schweiger, M.; Watzke, R.; Peschke, A.; Kappert, H. Ceramics as biomaterials for dental restoration. *Expert Rev. Med. Devices* **2008**, *5*, 729–745. [\[CrossRef\]](#) [\[PubMed\]](#)
8. Nevelos, J.E.; Ingham, E.; Doyle, C.; Nevelos, A.B.; Fisher, J. The influence of acetabular cup angle on the wear of “BIOLOX Forte” alumina ceramic bearing couples in a hip joint simulator. *J. Mater. Sci. Mater. Med.* **2001**, *12*, 141–144. [\[CrossRef\]](#) [\[PubMed\]](#)
9. Miracle, D.B. Metal matrix composites—From science to technological significance. *Compos. Sci. Technol.* **2005**, *65*, 2526–2540. [\[CrossRef\]](#)
10. Kurtz, A.D.; Mallon, J., Jr.; Nunn, T.A. Transducer structures employing ceramic substrates and diaphragms. U.S. Patent US4481497A, 6 11 1984.
11. He, X.; Zhang, A.Y.Z.; Mansell, A.J.P.; Su, A.B. Zirconia toughened alumina ceramic foams for potential bone graft applications: Fabrication, bioactivation, and cellular responses. *J. Mater. Sci. Mater. Med.* **2008**, *19*, 2743–2749. [\[CrossRef\]](#)
12. Mandal, N.; Doloi, B.; Mondal, B. Predictive modeling of surface roughness in high speed machining of AISI 4340 steel using yttria stabilized zirconia toughened alumina turning insert. *Int. J. Refract. Met. Hard Mater.* **2013**, *38*, 40–46. [\[CrossRef\]](#)
13. Oane, M.; Mahmood, M.A.; Popescu, A.C.; Banica, A.; Ristoscu, C.; Mihailescu, I.N. Thermal nonlinear klein-gordon equation for nano-micro-sized metallic particle-attosecond laser pulse interaction. *Materials* **2021**, *14*, 857. [\[CrossRef\]](#)
14. Bansal, N.P.; Boccaccini, A.R. *Ceramics and Composites Processing Methods*; John Wiley & Sons: Hoboken, NJ, USA, 2012; ISBN 9781118176658.
15. Zhang, B.; Zheng, X.L.; Tokura, H.; Yoshikawa, M. Grinding induced damage in ceramics. *J. Mater. Process. Technol.* **2003**, *132*, 353–364. [\[CrossRef\]](#)
16. Rosso, M. Ceramic and metal matrix composites: Routes and properties. *J. Mater. Process. Technol.* **2006**, *175*, 364–375. [\[CrossRef\]](#)
17. Zeng, W.M.; Li, Z.C.; Pei, Z.J.; Treadwell, C. Experimental observation of tool wear in rotary ultrasonic machining of advanced ceramics. *Int. J. Mach. Tools Manuf.* **2005**, *45*, 1468–1473. [\[CrossRef\]](#)
18. Mahmood, M.A.; Popescu, A.C.; Mihailescu, I.N. Metal Matrix Composites Synthesized by Laser-Melting Deposition: A Review. *Materials* **2020**, *13*, 2593. [\[CrossRef\]](#)
19. ASTM F2792 – 12a. *Stand. Terminol. Addit. Manuf. Technol.* **2013**, *10.04*. [\[CrossRef\]](#)
20. Ning, F.; Cong, W.; Hu, Y.; Wang, H. Additive manufacturing of carbon fiber-reinforced plastic composites using fused deposition modeling: Effects of process parameters on tensile properties. *J. Compos. Mater.* **2017**, *51*, 451–462. [\[CrossRef\]](#)
21. Huang, S.H.; Liu, P.; Mokasdar, A.; Hou, L. Additive manufacturing and its societal impact: A literature review. *Int. J. Adv. Manuf. Technol.* **2013**, *67*, 1191–1203. [\[CrossRef\]](#)
22. Prokhorov, A.M. *Laser Heating of Metals*; CRC Press: Boca Raton, FL, USA, 2018.
23. Bandyopadhyay, A.; Panda, R.K.; McNulty, T.F.; Mohammadi, F.; Danforth, S.C.; Safari, A. Piezoelectric ceramics and composites via rapid prototyping techniques. *Rapid Prototyp. J.* **1998**, *4*, 37–49. [\[CrossRef\]](#)
24. Bandyopadhyay, A.; Atisivan, R.; Kuhn, G.; Yeruva, S. Mechanical properties of interconnected phase alumina-Al composites. In Proceedings of the International Solid Freeform Fabrication Symposium, Austin, TX, USA, 7–9 August 2000; pp. 24–31.
25. Chartier, T.; Chaput, C.; Doreau, F.; Loiseau, M. Stereolithography of structural complex ceramic parts. *J. Mater. Sci.* **2002**, *37*, 3141–3147. [\[CrossRef\]](#)
26. Corcione, C.E.; Greco, A.; Montagna, F.; Licciulli, A.; Maffezzoli, A. Silica moulds built by stereolithography. *J. Mater. Sci.* **2005**, *40*, 4899–4904. [\[CrossRef\]](#)

27. Waetjen, A.M.; Polsakiewicz, D.A.; Kuhl, I.; Telle, R.; Fischer, H. Slurry deposition by airbrush for selective laser sintering of ceramic components. *J. Eur. Ceram. Soc.* **2009**, *29*, 1–6. [CrossRef]
28. Scheithauer, U.; Bergner, A.; Schwarzer, E.; Richter, H.J.; Moritz, T. Studies on thermoplastic 3D printing of steel-zirconia composites. *J. Mater. Res.* **2014**, *29*, 1931–1940. [CrossRef]
29. Klosterman, D.A.; Chartoff, R.P.; Osborne, N.R.; Graves, G.A.; Lightman, A.; Han, G.; Bezeredi, A.; Rodrigues, S. Development of a curved layer LOM process for monolithic ceramics and ceramic matrix composites. *Rapid Prototyp. J.* **1999**, *5*, 61–71. [CrossRef]
30. Bertrand, P.; Bayle, F.; Combe, C.; Goeuriot, P.; Smurov, I. Ceramic components manufacturing by selective laser sintering. *Appl. Surf. Sci.* **2007**, *254*, 989–992. [CrossRef]
31. Ghosh, S.K.; Saha, P. Crack and wear behavior of SiC particulate reinforced aluminium based metal matrix composite fabricated by direct metal laser sintering process. *Mater. Des.* **2011**, *32*, 139–145. [CrossRef]
32. Attar, H.; Bönisch, M.; Calin, M.; Zhang, L.C.; Scudino, S.; Eckert, J. Selective laser melting of in situ titanium-titanium boride composites: Processing, microstructure and mechanical properties. *Acta Mater.* **2014**, *76*, 13–22. [CrossRef]
33. Wilkes, J.; Hagedorn, Y.C.; Meiners, W.; Wissenbach, K. Additive manufacturing of ZrO₂-Al₂O₃ ceramic components by selective laser melting. *Rapid Prototyp. J.* **2013**, *19*, 51–57. [CrossRef]
34. Borkar, T.; Gopagani, S.; Nag, S.; Hwang, J.Y.; Collins, P.C.; Banerjee, R. In situ nitridation of titanium-molybdenum alloys during laser deposition. *J. Mater. Sci.* **2012**, *47*, 7157–7166. [CrossRef]
35. Balla, V.K.; Bose, S.; Bandyopadhyay, A. Processing of bulk alumina ceramics using laser engineered net shaping. *Int. J. Appl. Ceram. Technol.* **2008**, *5*, 234–242. [CrossRef]
36. Li, Y.; Hu, Y.; Cong, W.; Zhi, L.; Guo, Z. Additive manufacturing of alumina using laser engineered net shaping: Effects of deposition variables. *Ceram. Int.* **2017**, *43*, 7768–7775. [CrossRef]
37. Hu, Y.; Ning, F.; Wang, H.; Cong, W.; Zhao, B. Laser engineered net shaping of quasi-continuous network microstructural TiB reinforced titanium matrix bulk composites: Microstructure and wear performance. *Opt. Laser Technol.* **2018**, *99*, 174–183. [CrossRef]
38. Lee, H.; Lim, C.H.J.; Low, M.J.; Tham, N.; Murukeshan, V.M.; Kim, Y.J. Lasers in additive manufacturing: A review. *Int. J. Precis. Eng. Manuf. - Green Technol.* **2017**, *4*, 307–322. [CrossRef]
39. Kruth, J.P.; Levy, G.; Klocke, F.; Childs, T.H.C. Consolidation phenomena in laser and powder-bed based layered manufacturing. *CIRP Ann. - Manuf. Technol.* **2007**, *56*, 730–759. [CrossRef]
40. Hu, Y.; Li, J. Selective laser alloying of elemental titanium and boron powder: Thermal models and experiment verification. *J. Mater. Process. Technol.* **2017**, *249*, 426–432. [CrossRef]
41. Balla, V.K.; Bandyopadhyay, P.P.; Bose, S.; Bandyopadhyay, A. Compositionally graded yttria-stabilized zirconia coating on stainless steel using laser engineered net shaping (LENSTM). *Scr. Mater.* **2007**, *57*, 861–864. [CrossRef]
42. Hu, Y.; Wang, H.; Ning, F.; Cong, W. *Laser Engineered net Shaping of Commercially Pure Titanium: Effects of Fabricating Variables*; ASME International: New York, NY, USA, 2016.
43. Gu, D.D.; Meiners, W.; Wissenbach, K.; Poprawe, R. Laser additive manufacturing of metallic components: Materials, processes and mechanisms. *Int. Mater. Rev.* **2012**, *57*, 133–164. [CrossRef]
44. Weng, F.; Chen, C.; Yu, H. Research status of laser cladding on titanium and its alloys: A review. *Mater. Des.* **2014**, *58*, 412–425. [CrossRef]
45. Wu, Q.; Li, W.; Zhong, N.; Gang, W.; Haishan, W. Microstructure and wear behavior of laser cladding VC-Cr₇C₃ ceramic coating on steel substrate. *Mater. Des.* **2013**, *49*, 10–18. [CrossRef]
46. Emamian, A.; Corbin, S.F.; Khajepour, A. Effect of laser cladding process parameters on clad quality and in-situ formed microstructure of Fe-TiC composite coatings. *Surf. Coatings Technol.* **2010**, *205*, 2007–2015. [CrossRef]
47. Gao, Y.L.; Wang, C.S.; Yao, M.; Liu, H. bin The resistance to wear and corrosion of laser-cladding Al₂O₃ ceramic coating on Mg alloy. *Appl. Surf. Sci.* **2007**, *253*, 5306–5311. [CrossRef]
48. Weidong, Z.; Qibin, L.; Min, Z.; Xudong, W. Biocompatibility of a functionally graded bioceramic coating made by wide-band laser cladding. *J. Biomed. Mater. Res. Part A* **2008**, *87A*, 429–433. [CrossRef]
49. Wu, D.; Guo, M.; Ma, G.; Niu, F. Dilution characteristics of ultrasonic assisted laser clad yttria-stabilized zirconia coating. *Mater. Lett.* **2015**, *141*, 207–209. [CrossRef]
50. Alumina Chemical Compound Britannica. Available online: <https://www.britannica.com/science/alumina> (accessed on 22 July 2020).
51. Balakrishnan, P.; Thomas, S. Inert ceramics. In *Fundamental Biomaterials: Ceramics*; Elsevier Inc.: Amsterdam, The Netherlands, 2018; pp. 117–127. ISBN 9780081022047.
52. Wu, D.; Sun, B.; Niu, F.; Ma, G.; Zhang, Y.; Jin, Z. Microstructure and crack in color Al₂O₃ samples by laser engineered net shaping. *Kuei Suan Jen Hsueh Pao J. Chin. Ceram. Soc.* **2013**, *41*, 1621–1626. [CrossRef]
53. Niu, F.; Wu, D.; Zhou, S.; Ma, G. Power prediction for laser engineered net shaping of Al₂O₃ ceramic parts. *J. Eur. Ceram. Soc.* **2014**, *34*, 3811–3817. [CrossRef]
54. Huang, Y.; Wu, D.; Zhao, D.; Niu, F.; Zhang, H.; Yan, S.; Ma, G. Process optimization of melt growth alumina/aluminum titanate composites directed energy deposition: Effects of scanning speed. *Addit. Manuf.* **2020**, *35*, 101210. [CrossRef]
55. Dorozhkin, S. Calcium Orthophosphate Cements and Concretes. *Materials* **2009**, *2*, 221–291. [CrossRef]

56. Xia, L.; Lin, K.; Jiang, X.; Xu, Y.; Zhang, M.; Chang, J.; Zhang, Z. Enhanced osteogenesis through nano-structured surface design of macroporous hydroxyapatite bioceramic scaffolds via activation of ERK and p38 MAPK signaling pathways. *J. Mater. Chem. B* **2013**, *1*, 5403–5416. [[CrossRef](#)] [[PubMed](#)]
57. Tabrizian, M. Expression of concern: Nanodimensional and Nanocrystalline apatites and other calcium orthophosphates in biomedical engineering, biology and medicine. *Materials* **2009**, *2*, 1975–2045. *Materials* **2016**, *9*, 752. [[CrossRef](#)]
58. Vallet-Regí, M.; González-Calbet, J.M. Calcium phosphates as substitution of bone tissues. *Prog. Solid State Chem.* **2004**, *32*, 1–31. [[CrossRef](#)]
59. Okabayashi, R.; Nakamura, M.; Okabayashi, T.; Tanaka, Y.; Nagai, A.; Yamashita, K. Efficacy of polarized hydroxyapatite and silk fibroin composite dressing gel on epidermal recovery from full-thickness skin wounds. *J. Biomed. Mater. Res. Part B Appl. Biomater.* **2009**, *90B*, 641–646. [[CrossRef](#)] [[PubMed](#)]
60. Shin, Y.; Aoki, H.; Yoshiyama, N.; Akao, M.; Higashikata, M. Surface properties of hydroxyapatite ceramic as new percutaneous material in skin tissue. *J. Mater. Sci. Mater. Med.* **1992**, *3*, 219–221. [[CrossRef](#)]
61. Ji, D.Y.; Kuo, T.F.; Wu, H.D.; Yang, J.C.; Lee, S.Y. A novel injectable chitosan/polyglutamate polyelectrolyte complex hydrogel with hydroxyapatite for soft-tissue augmentation. *Carbohydr. Polym.* **2012**, *89*, 1123–1130. [[CrossRef](#)]
62. Liu, M.; Zhou, G.; Song, W.; Li, P.; Liu, H.; Niu, X.; Fan, Y. Effect of nano-hydroxyapatite on the axonal guidance growth of rat cortical neurons. *Nanoscale* **2012**, *4*, 3201–3207. [[CrossRef](#)]
63. Uskoković, V.; Uskoković, D.P. Nanosized hydroxyapatite and other calcium phosphates: Chemistry of formation and application as drug and gene delivery agents. *J. Biomed. Mater. Res. Part B Appl. Biomater.* **2011**, *96 B*, 152–191. [[CrossRef](#)]
64. Rodríguez-Ruiz, I.; Delgado-López, J.M.; Durán-Olivencia, M.A.; Iafisco, M.; Tampieri, A.; Colangelo, D.; Prat, M.; Gómez-Morales, J. PH-responsive delivery of doxorubicin from citrate-apatite nanocrystals with tailored carbonate content. *Langmuir* **2013**, *29*, 8213–8221. [[CrossRef](#)]
65. Lin, K.; Liu, P.; Wei, L.; Zou, Z.; Zhang, W.; Qian, Y.; Shen, Y.; Chang, J. Strontium substituted hydroxyapatite porous microspheres: Surfactant-free hydrothermal synthesis, enhanced biological response and sustained drug release. *Chem. Eng. J.* **2013**, *222*, 49–59. [[CrossRef](#)]
66. Lin, K.; Chen, L.; Liu, P.; Zou, Z.; Zhang, M.; Shen, Y.; Qiao, Y.; Liu, X.; Chang, J. Hollow magnetic hydroxyapatite microspheres with hierarchically mesoporous microstructure for pH-responsive drug delivery. *CrystEngComm* **2013**, *15*, 2999–3008. [[CrossRef](#)]
67. Zhu, S.H.; Huang, B.Y.; Zhou, K.C.; Huang, S.P.; Liu, F.; Li, Y.M.; Xue, Z.G.; Long, Z.G. Hydroxyapatite nanoparticles as a novel gene carrier. *J. Nanoparticle Res.* **2004**, *6*, 307–311. [[CrossRef](#)]
68. Li, J.; Chen, Y.C.; Tseng, Y.C.; Mozumdar, S.; Huang, L. Biodegradable calcium phosphate nanoparticle with lipid coating for systemic siRNA delivery. *J. Control. Release* **2010**, *142*, 416–421. [[CrossRef](#)]
69. Hilbrig, F.; Freitag, R. Isolation and purification of recombinant proteins, antibodies and plasmid DNA with hydroxyapatite chromatography. *Biotechnol. J.* **2012**, *7*, 90–102. [[CrossRef](#)]
70. Morrison, C.J.; Gagnon, P.; Cramer, S.M. Purification of monomeric mAb from associated aggregates using selective desorption chromatography in hydroxyapatite systems. *Biotechnol. Bioeng.* **2011**, *108*, 813–821. [[CrossRef](#)]
71. Kozlova, D.; Chernousova, S.; Knuschke, T.; Buer, J.; Westendorf, A.M.; Eppel, M. Cell targeting by antibody-functionalized calcium phosphate nanoparticles. *J. Mater. Chem.* **2012**, *22*, 396–404. [[CrossRef](#)]
72. Chen, F.; Huang, P.; Zhu, Y.J.; Wu, J.; Cui, D.X. Multifunctional Eu³⁺/Gd³⁺ dual-doped calcium phosphate vesicle-like nanospheres for sustained drug release and imaging. *Biomaterials* **2012**, *33*, 6447–6455. [[CrossRef](#)]
73. Eppel, M.; Ganesan, K.; Heumann, R.; Klesing, J.; Kovtun, A.; Neumann, S.; Sokolova, V. Application of calcium phosphate nanoparticles in biomedicine. *J. Mater. Chem.* **2010**, *20*, 18–23. [[CrossRef](#)]
74. Totleng, M.; Akinlabi, E.; Shukla, M.; Pityana, S. Microstructures, hardness and bioactivity of hydroxyapatite coatings deposited by direct laser melting process. *Mater. Sci. Eng. C* **2014**, *43*, 189–198. [[CrossRef](#)]
75. Du, H.; Huo, W.; Gao, H.; Wang, L.; Qiu, S.; Liu, J. Influence of Zirconia on Hydroxyapatite Coating on Ti-Alloy by Laser Cladding. *J. Tianjin Univ. English Ed.* **2003**, *9*, 292–295.
76. Zeng, H.; Lacefield, W.R. The study of surface transformation of pulsed laser deposited hydroxyapatite coatings. *J. Biomed. Mater. Res.* **2000**, *50*, 239–247. [[CrossRef](#)]
77. Hasan, M.F.; Wang, J.; Berndt, C.C. Effect of power and stand-off distance on plasma sprayed hydroxyapatite coatings. *Mater. Manuf. Process.* **2013**, *28*, 1279–1285. [[CrossRef](#)]
78. Farid, S.B.H. Structure, microstructure, and properties of bioceramics. In *Bioceramics: For Materials Science and Engineering*; Elsevier: Amsterdam, The Netherlands, 2019; pp. 39–76.
79. Gutknecht, D.; Chevalier, J.; Garnier, V.; Fantozzi, G. Key role of processing to avoid low temperature ageing in alumina zirconia composites for orthopaedic application. *J. Eur. Ceram. Soc.* **2007**, *27*, 1547–1552. [[CrossRef](#)]
80. Ganesh, I.; Olhero, S.M.; Torres, P.M.C.; Alves, F.J.; Ferreira, J.M.F. Hydrolysis-induced aqueous gelcasting for near-net shape forming of ZTA ceramic composites. *J. Eur. Ceram. Soc.* **2009**, *29*, 1393–1401. [[CrossRef](#)]
81. Wang, J.; Stevens, R. Zirconia-toughened alumina (ZTA) ceramics. *J. Mater. Sci.* **1989**, *24*, 3421–3440. [[CrossRef](#)]
82. Denry, I.; Kelly, J.R. State of the art of zirconia for dental applications. *Dent. Mater.* **2008**, *24*, 299–307. [[CrossRef](#)]
83. Yan, S.; Wu, D.; Niu, F.; Ma, G.; Kang, R. Al₂O₃-ZrO₂ eutectic ceramic via ultrasonic-assisted laser engineered net shaping. *Ceram. Int.* **2017**, *43*, 15905–15910. [[CrossRef](#)]

84. Hu, Y.; Wang, H.; Cong, W.; Zhao, B. Directed energy deposition of zirconia-toughened alumina ceramic: Novel microstructure formation and mechanical performance. *J. Manuf. Sci. Eng.* **2020**, *142*. [\[CrossRef\]](#)
85. Harris, G.L. *PROPERTIES OF Silicon Carbide*; INSPEC, The Institution of Electrical Engineers: London, UK, 1995; ISBN 0852968701.
86. Ji, R.; Liu, Y.; Zhang, Y.; Cai, B.; Li, X.; Zheng, C. Effect of machining parameters on surface integrity of silicon carbide ceramic using end electric discharge milling and mechanical grinding hybrid machining. *J. Mech. Sci. Technol.* **2013**, *27*, 177–183. [\[CrossRef\]](#)
87. Adebisi, I.; Fatoba, O.; Pityana, S.; Popoola, P. Parameters Optimization, Microstructure and Micro-Hardness of Silicon Carbide Laser Deposited on Titanium Alloy. In Proceedings of the International Conference on Surface Modification Technologies, Milan, Italy, 29 June–1 July 2016.
88. Dutta Majumdar, J.; Ramesh Chandra, B.; Nath, A.K.; Manna, I. Studies on compositionally graded silicon carbide dispersed composite surface on mild steel developed by laser surface cladding. *J. Mater. Process. Technol.* **2008**, *203*, 505–512. [\[CrossRef\]](#)
89. Lusquiños, F.; Pou, J.; Quintero, F.; Pérez-Amor, M. Laser cladding of SiC/Si composite coating on Si-SiC ceramic substrates. *Surf. Coatings Technol.* **2008**, *202*, 1588–1593. [\[CrossRef\]](#)
90. Wang, H.M.; Yu, Y.L.; Li, S.Q. Microstructure and tribological properties of laser clad CaF₂/Al₂O₃ self-lubrication wear-resistant ceramic matrix composite coatings. *Scr. Mater.* **2002**, *47*, 57–61. [\[CrossRef\]](#)
91. Xu, X.; Han, J.; Wang, C.; Huang, A. Laser cladding of composite bioceramic coatings on titanium alloy. *J. Mater. Eng. Perform.* **2016**, *25*, 656–667. [\[CrossRef\]](#)
92. Roy, M.; Vamsi Krishna, B.; Bandyopadhyay, A.; Bose, S. Laser processing of bioactive tricalcium phosphate coating on titanium for load-bearing implants. *Acta Biomater.* **2008**, *4*, 324–333. [\[CrossRef\]](#) [\[PubMed\]](#)
93. Khanna, A.S.; Kumari, S.; Kanungo, S.; Gasser, A. Hard coatings based on thermal spray and laser cladding. *Int. J. Refract. Met. Hard Mater.* **2009**, *27*, 485–491. [\[CrossRef\]](#)
94. Kumar, B.K.A.G.; Ananthaprasad, M.; GopalaKrishna, K. A review on mechanical and tribological behaviors of nickel matrix composites. *Indian J. Sci. Technol.* **2016**, *9*, 1–7. [\[CrossRef\]](#)
95. Gopagani, S.; Hwang, J.Y.; Singh, A.R.P.; Mensah, B.A.; Bunce, N.; Tiley, J.; Scharf, T.W.; Banerjee, R. Microstructural evolution in laser deposited nickel-titanium-carbon in situ metal matrix composites. *J. Alloys Compd.* **2011**, *509*, 1255–1260. [\[CrossRef\]](#)
96. Li, Y.; Bai, P.; Wang, Y.; Hu, J.; Guo, Z. Effect of TiC content on Ni/TiC composites by direct laser fabrication. *Mater. Des.* **2009**, *30*, 1409–1412. [\[CrossRef\]](#)
97. Hong, C.; Gu, D.; Dai, D.; Alkhayat, M.; Urban, W.; Yuan, P.; Cao, S.; Gasser, A.; Weisheit, A.; Kelbassa, I.; et al. Laser additive manufacturing of ultrafine TiC particle reinforced Inconel 625 based composite parts: Tailored microstructures and enhanced performance. *Mater. Sci. Eng. A* **2015**, *635*, 118–128. [\[CrossRef\]](#)
98. Li, X.C.; Stampfl, J.; Prinz, F.B. Mechanical and thermal expansion behavior of laser deposited metal matrix composites of Invar and TiC. *Mater. Sci. Eng. A* **2000**, *282*, 86–90. [\[CrossRef\]](#)
99. Liu, D.; Zhang, S.Q.; Li, A.; Wang, H.M. Microstructure and tensile properties of laser melting deposited TiC/TA15 titanium matrix composites. *J. Alloys Compd.* **2009**, *485*, 156–162. [\[CrossRef\]](#)
100. Mahamood, R.M.; Akinlabi, E.T.; Shukla, M.; Pityana, S. Scanning velocity influence on microstructure, microhardness and wear resistance performance of laser deposited Ti6Al4V/TiC composite. *Mater. Des.* **2013**, *50*, 656–666. [\[CrossRef\]](#)
101. Tamirisakandala, S.; Miracle, D.B.; Srinivasan, R.; Gunasekera, J.S. Titanium Alloyed with Boron. *Adv. Mater. Process.* **2006**, *164*, 41.
102. Ochonogor, O.F.; Meacock, C.; Pityana, S.L.; Popoola, P.A.I.; Majumder, J.D. Microstructure characterization of laser-deposited titanium carbide and zirconium-based titanium metal matrix composites. *J. South. African Inst. Min. Metall.* **2012**, *112*, 905–910.
103. Das, M.; Balla, V.K.; Basu, D.; Manna, I.; Sampath Kumar, T.S.; Bandyopadhyay, A. Laser processing of in situ synthesized TiB-TiN-reinforced Ti6Al4V alloy coatings. *Scr. Mater.* **2012**, *66*, 578–581. [\[CrossRef\]](#)
104. Van Acker, K.; Vanhoyweghen, D.; Persoons, R.; Vangrunderbeek, J. Influence of tungsten carbide particle size and distribution on the wear resistance of laser clad WC/Ni coatings. In *Proceedings of the Wear*; Elsevier: Amsterdam, The Netherlands, 2005; Volume 258, pp. 194–202.
105. Das, M.; Balla, V.K.; Kumar, T.S.S.; Manna, I. Fabrication of Biomedical Implants using Laser Engineered Net Shaping (LENSTM). *Trans. Indian Ceram. Soc.* **2013**, *72*, 169–174. [\[CrossRef\]](#)
106. Balla, V.K.; Bhat, A.; Bose, S.; Bandyopadhyay, A. Laser processed TiN reinforced Ti6Al4V composite coatings. *J. Mech. Behav. Biomed. Mater.* **2012**, *6*, 9–20. [\[CrossRef\]](#) [\[PubMed\]](#)
107. Das, M.; Balla, V.K.; Kumar, T.S.S.; Bandyopadhyay, A.; Manna, I. Tribological, electrochemical and in vitro biocompatibility properties of SiC reinforced composite coatings. *Mater. Des.* **2016**, *95*, 510–517. [\[CrossRef\]](#)
108. Acharya, R.; Sharon, J.A.; Staroselsky, A. Prediction of microstructure in laser powder bed fusion process. *Acta Mater.* **2017**, *124*, 360–371. [\[CrossRef\]](#)
109. Fergani, O.; Berto, F.; Welo, T.; Liang, S.Y. Analytical modelling of residual stress in additive manufacturing. *Fatigue Fract. Eng. Mater. Struct.* **2017**, *40*, 971–978. [\[CrossRef\]](#)
110. Chen, Q.; Guillemot, G.; Gandin, C.A.; Bellet, M. Three-dimensional finite element thermomechanical modeling of additive manufacturing by selective laser melting for ceramic materials. *Addit. Manuf.* **2017**, *16*, 124–137. [\[CrossRef\]](#)
111. Yu, T.; Li, M.; Breaux, A.; Atri, M.; Obeidat, S.; Ma, C. Experimental and numerical study on residual stress and geometric distortion in powder bed fusion process. *J. Manuf. Process.* **2019**, *46*, 214–224. [\[CrossRef\]](#)

112. Mahmood, M.A.; Popescu, A.C.; Hapenciuc, C.L.; Ristoscu, C.; Visan, A.I.; Oane, M.; Mihailescu, I.N. Estimation of clad geometry and corresponding residual stress distribution in laser melting deposition: Analytical modeling and experimental correlations. *Int. J. Adv. Manuf. Technol.* **2020**, *111*, 77–91. [\[CrossRef\]](#)
113. Mahmood, M.A.; Popescu, A.C.; Oane, M.; Ristoscu, C.; Chioibas, D.; Mihai, S.; Mihailescu, I.N. Three-jet powder flow and laser–powder interaction in laser melting deposition: Modelling versus experimental correlations. *Metals* **2020**, *10*, 1113. [\[CrossRef\]](#)
114. Arif, M.; Popescu, A.C.; Oane, M.; Chioibas, D.; Popescu-pelin, G.; Ristoscu, C.; Mihailescu, I.N. Grain refinement and mechanical properties for AISI304 stainless steel single-tracks by laser melting deposition: Mathematical modelling versus experimental results. *Results Phys.* **2021**, *22*, 103880. [\[CrossRef\]](#)
115. Buc, A.M.; Oane, M.; Mahmood, M.A.; Mih, I.N.; Popescu, A.C.; Sava, B.A.; Ristoscu, C. Non-fourier estimate of electron temperature in case of femtosecond laser pulses interaction with metals. *Metals* **2020**, *10*, 606. [\[CrossRef\]](#)
116. Asif, U.R.; Sglavo, V.M. 3D printing of geopolymer-based concrete for building applications. *Rapid prot.* **2020**, *26*, 1783–1788. [\[CrossRef\]](#)
117. Mahmood, M.A.; Han, C.F.; Chu, H.Y.; Sun, C.C.; Wu, W.H.; Lin, W.J.; Liu, L.C.; Lai, J.Y.; Mihailescu, I.N.; Lin, J.F. Effects of roll pattern and reduction ratio on optical characteristics of A1008 cold-rolled steel specimens: Analytical approach and experimental correlations. *Int. J. Adv. Manuf. Technol.* **2020**, *111*, 2001–2020. [\[CrossRef\]](#)
118. Mahmood, M.A.; Tsai, T.Y.; Hwu, Y.J.; Lin, W.J.; Liu, L.C.; Lai, J.Y.; Pan, J.W.; Li, W.L.; Lin, J.F. Effect of fractal parameters on optical properties of cold rolled aluminum alloy strips with induced surface deflection: Simulations and experimental correlations. *J. Mater. Process. Technol.* **2020**, *279*, 116554. [\[CrossRef\]](#)
119. Bucă, A.M.; Oane, M.; Mihailescu, I.N.; Mahmood, M.A.; Sava, B.A.; Ristoscu, C. An analytical multiple-temperature model for flash laser irradiation on single-layer graphene. *Nanomaterials* **2020**, *10*, 1319. [\[CrossRef\]](#)
120. Mahmood, M.A.; Visan, A.I.; Ristoscu, C.; Mihailescu, I.N. Artificial neural network algorithms for 3D printing. *Materials* **2021**, *14*, 163. [\[CrossRef\]](#) [\[PubMed\]](#)
121. Sayyad Amin, J.; Nikooee, E.; Ayatollahi, S.; Alamdari, A. Investigating wettability alteration due to asphaltene precipitation: Imprints in surface multifractal characteristics. *Appl. Surf. Sci.* **2010**, *256*, 6466–6472. [\[CrossRef\]](#)
122. Yang, Y.; Lan, J.; Li, X. Study on bulk aluminum matrix nano-composite fabricated by ultrasonic dispersion of nano-sized SiC particles in molten aluminum alloy. *Mater. Sci. Eng. A* **2004**, *380*, 378–383. [\[CrossRef\]](#)
123. Ning, F.; Hu, Y.; Liu, Z.; Wang, X.; Li, Y.; Cong, W. Ultrasonic vibration-assisted laser engineered net shaping of inconel 718 Parts: Microstructural and mechanical characterization. *J. Manuf. Sci. Eng. Trans. ASME* **2018**, *140*. [\[CrossRef\]](#)
124. Abramov, O.V. Action of high intensity ultrasound on solidifying metal. *Ultrasonics* **1987**, *25*, 73–82. [\[CrossRef\]](#)
125. Cong, W.; Ning, F. A fundamental investigation on ultrasonic vibration-assisted laser engineered net shaping of stainless steel. *Int. J. Mach. Tools Manuf.* **2017**, *121*, 61–69. [\[CrossRef\]](#)
126. Moraru, L. Ultrasound action on strength properties of polycrystalline metals. In *The Annals of University “Dunărea De Jos” of Galați Fascicle VIII*; Galati University Press: Galati, Romania, 2006; pp. 73–76.
127. Munz, D.; Fett, T. *Ceramics: Mechanical Properties, Failure Behaviour, Materials Selection Illustrate*; Springer Science & Business Media: Berlin/Heidelberg, Germany, 1999; ISBN 9783540653769.
128. Quazi, M.M.; Fazal, M.A.; Haseeb, A.S.M.A.; Yusof, F.; Masjuki, H.H.; Arslan, A. Effect of rare earth elements and their oxides on tribo-mechanical performance of laser claddings: A review. *J. Rare Earths* **2016**, *34*, 549–564. [\[CrossRef\]](#)
129. Zhou, S.; Huang, Y.; Zeng, X.; Hu, Q. Microstructure characteristics of Ni-based WC composite coatings by laser induction hybrid rapid cladding. *Mater. Sci. Eng. A* **2008**, *480*, 564–572. [\[CrossRef\]](#)
130. Triantafyllidis, D.; Li, L.; Stott, F.H. Crack-free densification of ceramics by laser surface treatment. *Surf. Coatings Technol.* **2006**, *201*, 3163–3173. [\[CrossRef\]](#)
131. Hu, Y.; Zhao, B.; Ning, F.; Wang, H.; Cong, W. In-situ ultrafine three-dimensional quasi-continuous network microstructural TiB reinforced titanium matrix composites fabrication using laser engineered net shaping. *Mater. Lett.* **2017**, *195*, 116–119. [\[CrossRef\]](#)
132. Huang, L.J.; Geng, L.; Peng, H.X. Microstructurally inhomogeneous composites: Is a homogeneous reinforcement distribution optimal? *Prog. Mater. Sci.* **2015**, *71*, 93–168. [\[CrossRef\]](#)